The Version of Record of this manuscript has been published and is available in The Journal of Adhesion in press https://doi.org/10.1080/00218464.2019.1665519

Effect of temperature on cohesive modelling of 3M Scotch-Weld™ 7260 B/A epoxy adhesive

A. Bernasconi[1,*], R.A.A. Lima[1], S. Cardamone[1], R.B. Campbell[2], A. Slocum[2], M. Giglio[1]

[1]Dipartimento di Meccanica, Politecnico di Milano, Milan, Italy.

[2]Department of Mechanical Engineering, MIT, Cambridge (MA) USA

[*] Corresponding author: andrea.bernasconi@polimi.it

This work addresses the effect of the test temperature on the cohesive model parameters for the 3M Scotch-Weld™ 7260 B/A epoxy adhesive. It extends a previous experimental work done at room temperature and further develops a previously proposed parameter identification method based on optimization. Double-Cantilever Beam (DCB) and End-Notched Flexure (ENF) tests were conducted at four different temperatures: 20°C, 40°C, 55°C and 70°C. Moreover, Single Lap Joints (SLJ), and bulk specimens' tensile tests were carried out. Finite element analyses of DCB and ENF tests were performed and optimization algorithms were used to calculate constitutive cohesive model parameters. Three approaches were followed. First, cohesive parameters were derived from bulk tests. Then, optimization with two variables for each mode was conducted, to identify the parameters e_i and $\sigma_{u,i}$ (i=I, II) of a triangular traction separation law. In the third, only $\sigma_{u,i}$, was taken as variable, while e_i was derived from the elastic modulus of the bulk adhesive. Finally, the cohesive models were applied to simulate the response of the SLJ, and numerical results were compared with experiments. The two free variables optimization method allowed to obtain the most accurate predictions of the maximum load and SLJ displacement at failure.

Keywords: Numerical optimization, temperature effects, cohesive parameters identification., epoxy/epoxides < Adhesive materials, mechanical properties of adhesives < Phenomena, fracture mechanics < Methods of analysis

The Version of Record of this manuscript has been published and is available in The Journal of Adhesion in press https://doi.org/10.1080/00218464.2019.1665519

1. INTRODUCTION

In the recent decades, the use of adhesives to replace conventional joining techniques has grown significantly because of their advantages, such as better stress distribution, reduction of final product weight and ease of joining different materials. However, some limitations arise from the dependence of their mechanical properties on environmental conditions, the possible difference between their Coefficient of Thermal Expansion (CTE) and that of the substrate and the complexity of predicting their strength and failure behaviour [1]– [11] . In this paper, the dependence on temperature of the mechanical behaviour of an epoxy adhesive, previously studied at room temperature [12], is investigated and the impact of temperature on the parameters of cohesive zone models is assessed.

The influence of temperature variations on the mechanical and fracture behaviour of the adhesive joints has been studied in [2], [4]– [6] and [8]–[16]. A. Deb *et al*. 2008 [4], analysed experimentally the behaviour of Double Lap Shear (DLS) at three different temperatures -20°C, room temperature and 82°C. It was observed that increasing temperature corresponds to a decrease of the adhesive strength.

Banea *et al.* [9] studied the effect of temperature on the shear strength of aluminium Single Lap Joints (SLJ) for high temperatures applications. Tensile tests were performed at different temperatures (room temperature, 100, 150, 200°C) and numerical predictions were obtained using a bilinear traction separation law. It was found that the allowable lap shear stress increased with the adhesive ductility and bulk strength. However, for temperatures above the T_g the lap shear strength decreased.

The Version of Record of this manuscript has been published and is available in The Journal of Adhesion in press https://doi.org/10.1080/00218464.2019.1665519

Fernandes *et al*. [15] investigated temperature effects on pure modes I and II fracture behaviour of composite bonded joints at 0°C, 20°C and 50°C. In mode I, at the first two temperatures similar values of the fracture toughness were obtained, followed by a huge reduction at 50°C. Otherwise, the fracture energy in pure mode II did not show significative changes with temperature variations.

In order to predict the strength of adhesive joints, different numerical techniques were proposed, based on the Finite Elements Method (FEM). Stress/strain or fracture mechanics criteria [17], Linear Elastic Fracture Mechanics (LEFM) trough the Virtual Crack Closure Technique (VCCT) [18], [19] and, more recently, the Cohesive Zone Methods (CZM) have been used to predict the mechanical behaviour of adhesive joints and composite materials. The CZM allows damage growth simulation combining stress-based analysis and fracture mechanics trough the implementation of softening relationships called Traction Separation Laws (TSL) [8], [20]– [23]. The CZM is particularly suitable for strength prediction of adhesive joints due to the possibility of using different TSL shapes selected in base of the adhesive characteristics [20], [21], [23], [24], as the bilinear (triangular), exponential and trilinear (trapezoidal) shapes.

Campilho *et al*. [19], evaluated the effect of three different cohesive law shapes (triangular, exponential and trapezoidal) in the numerical simulations of the mechanical behaviour of single lap joints. Two different adhesives were used, a high strength and brittle one (Araldite AV138) and a ductile adhesive (Araldite 2015). It was found that for brittle adhesives the CZM shape does not affect the accuracy of the numerical results. On the other hand, for ductile adhesives the plastic behaviour of the adhesive at the end of the

The Version of Record of this manuscript has been published and is available in The Journal of Adhesion in press https://doi.org/10.1080/00218464.2019.1665519

elastic zone and, consequently, the prediction of the bonded joint strength were best described by a trilinear TSL.

The use of a TSL requires accurate knowledge of the adhesive fracture path and materials properties such as the strain energy release rate (G_{IC} and G_{IIC}), the ultimate stress in tension and shear (t_I and t_{II}) and the initial stiffness parameters (e_I and e_{II}). Campilho *et al*. [20], studied the influence of cohesive parameters on the output of the SLJ simulations using a CZM with triangular TSL. The under prediction of the parameters G_{IC} and G_{IIC} resulted into a reduction of the accuracy of the numerical results of SLJ, except for the case of joints with extremely small overlap length. However, for over prediction of the critical strain energy release rate minor effects were found. Increasing the t_I values resulted into a negligible variation of the SLJ strength prediction, while a reduction of the t_I presented moderate effects.

Rocha and Campilho *et al*. [23] evaluated the influence of the elastic stiffness, mesh refinement, element type and damage initiation criterion in the CZM of single lap bonded joints. It was found that the stiffness parameter decreases its influence on the strength prediction as adhesive ductility increases. Moreover, mesh refinement did not present relevant effects in CZM.

Basically, three different approaches can be used to determine the parameters to be implemented in the TSL: properties calculation by specific experimental tests, inverse and direct methods. The inverse method estimates the CZM parameters by fitting the simulations output with the experimental results (typically by the loading-displacement

The Version of Record of this manuscript has been published and is available in The Journal of Adhesion in press https://doi.org/10.1080/00218464.2019.1665519

curve), while the direct method identifies the TSL shape from DCB and ENF fracture tests [8], [21], [22]- [25].

Qin *et al.* [26] proposed a failure prediction in function of the temperature of an adhesively bonded CFRP-aluminium alloy joints using an experimental-numerical approach. Bulk tensile tests and scarf joints were tested at -40, 23 and 80°C and CZM numerical analysis using a quadratic stress criterion and a bi-linear TSL were performed. The high temperature presented more important impact in the joint mechanical properties than the low temperature. The use of a quadratic stress criterion based on the experimental tests allowed for great accuracy on the prediction of failure modes.

In a previous work, Cardamone *et al*. [12] characterized the 3M Scotch-Weld 7260 B/A two-component epoxy resin by DCB and ENF tests at room temperature. In addition, the parameters of a bilinear CZM were determined by numerical optimization with two free variables for each mode (the ultimate stress and stiffness parameters in tension and shear) using the software Abaqus™ and Isigth™. Then, numerical simulations of a full-scale joint were done using the cohesive parameters determined by the numerical optimization. The results showed a good agreement between the numerical and experimental outputs at room temperature and confirmed the validation of the chosen CZM.

The aim of this work is to identify cohesive model parameters for the 3M Scotch-Weld™ 7260 B/A epoxy adhesive (3M, Saint Paul MN, USA) as a function of temperature. DCB and ENF tests at different temperatures (20°C – from [12], 40°C, 55°C and 70°C) were conducted. Then, bulk tensile tests were carried out in order to determine the effect of

The Version of Record of this manuscript has been published and is available in The Journal of Adhesion in press https://doi.org/10.1080/00218464.2019.1665519

temperature on the mechanical behaviour of the adhesive. Finally, SLJ were tested at the same temperatures.

Numerical optimizations were developed to determine the cohesive parameters of the studied adhesive on the basis of the fracture toughness identified by the DCB and ENF tests. Two numerical optimization strategies were applied: First, an extension of the two free variables method described in [12] was performed, Then, a new strategy was proposed using only one free variable of the bilinear TSL (the ultimate stress in shear and tension) while the other parameters (the critical strain energy release rate and the stiffness) were obtained from experimental tests (DCB, ENF and bulk tensile test). Cohesive parameters were also identified on the basis of bulk test results, for comparison purpose. Finally, numerical simulations were performed in Abaqus (Dassault Sistèmes, Vélizy-Villacoublay, France) using CZM, in order to predict the strength of the SLJ specimens at different temperatures.

2. METHODOLOGY

2.1. Materials

A high viscosity bi-component 3M Scotch-Weld^{TM} 7260 B/A (Non – Sag) epoxy was used. For the fabrication of each specimen the same polymerization procedure was applied. The curing process was divided in three main steps: continuous increasing of the temperature from room temperature up to 65°C (during 1:30 hour), followed by 3:30 hours at 65°C and finally, continuous cooling from 65°C to room temperature (during 1:00 hour).

The Version of Record of this manuscript has been published and is available in The Journal of Adhesion in press https://doi.org/10.1080/00218464.2019.1665519

Two different materials were used as substrates: a high-strength steel DIN 40 CrMoMn7 for the DCB and ENF specimens and a structural steel S355 for the SLJ. The substrates properties are reported in tables 1 and 2. The mechanical properties in table 2 were obtained through tensile tests of S355 plates with 1.5 mm of thickness, using an MTS electro-mechanical testing machine with a load cell of 150 kN and test speed of 2.5 mm/min.

Table 1: Mechanical properties of DIN 40 CrMoMn7 [1].

Tensile failure strength (MPa)	1000
Yield stress (MPa)	861
Elongation (%)	14-17
Young's modulus – E (MPa)	205000

Table 2: Mechanical properties of S355.

Tensile failure strength (MPa)	440-450
Yield stress (MPa)	380-420
Elongation (%)	25-35
Young's modulus – E (MPa)	207148

The Version of Record of this manuscript has been published and is available in The Journal of Adhesion in press https://doi.org/10.1080/00218464.2019.1665519

2.2. Specimens fabrication

2.2.1. DCB and ENF specimens

The geometry of the DCB specimen was defined according to the standard ASTM D3433, as can be seen in Figure 1. The ENF specimen was manufactured with the same dimensions and materials as of the DCB sample.

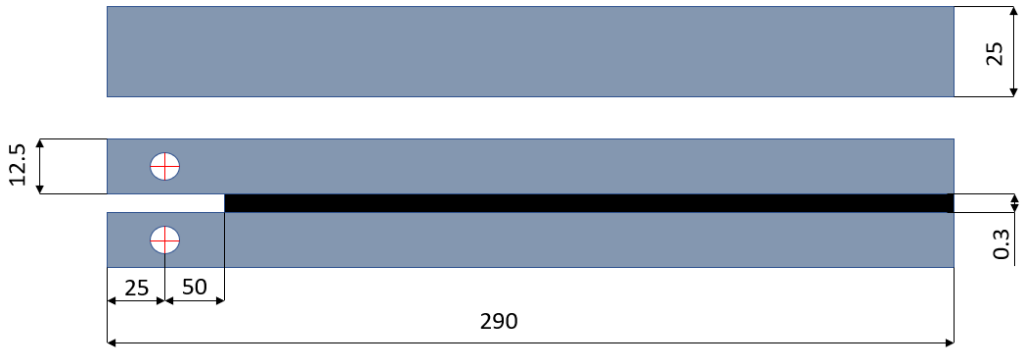

Figure 1: DCB and ENF dimensions in mm.

The substrates were sandblasted and degreased with acetone before the adhesive application to eliminate impurities. The adhesive bondline thickness was equal to 0.3 mm and in order to guarantee the specified thickness glass microspheres were used (concentration of 2% by weight of the adhesive). In the initial part of the samples a 0.1mm polytetrafluoroethylene (PTFE) tape was applied to avoid the presence of adhesive and reduce friction during the ENF test. Finally, a white spray was applied onto the adhesive line in order to facilitate the visualization of the crack propagation during the test.

The Version of Record of this manuscript has been published and is available in The Journal of Adhesion in press https://doi.org/10.1080/00218464.2019.1665519

2.2.2. Single lap joints

Plates of structural steel S355 were used as substrate of the SLJ samples. SLJ dimensions followed the ASTM D1002 standard, as can be seen in Fig. 2.

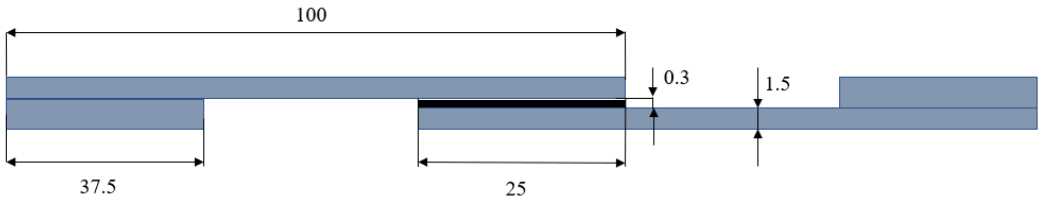

Figure 2: SLJ geometry - dimensions in mm.

The substrates were sandblasted and cleaned with acetone before bonding. As described for the ENF and DCB samples, glass microspheres were added to the adhesive line in order to maintain a nominal thickness equal to 0.3 mm. The overlap length was set to 25 mm. Steel tabs were bonded to the samples' ends to guarantee a correct alignment in the test machine.

2.2.3. *Bulk tensile test*

Thin adhesive plates were produced by curing the 7260 A/B epoxy adhesive in a metallic mould with a silicon frame as recommended by the French standard NF T 76 – 142. After the adhesive deposition in the mould, it was hot pressed at 65°C and 2 MPa for 3 hours. The final adhesive plate dimensions were 150 x 50mm and thickness equal to 3mm. The

The Version of Record of this manuscript has been published and is available in The Journal of Adhesion in press https://doi.org/10.1080/00218464.2019.1665519

adhesive plate was machined to manufacture dogbone samples identified as Type 1BB in the ISO 527 standard , as shown in Figure 3.

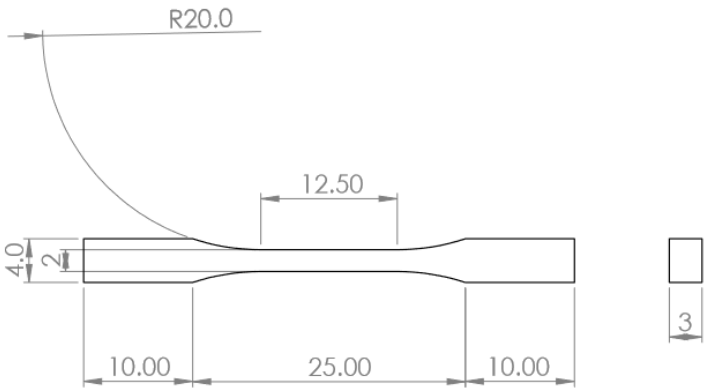

Figure 3: Bulk adhesive specimen - small dimensions.

2.3. Test procedures

2.3.1. DCB and ENF tests

The DCB and ENF samples were tested at room temperature (results from [12]), 40°C, 55°C and 70°C, using an MTS electro-mechanical testing machine with a load cell of 150 kN. The test speed was 0.5 mm/min as suggested by the ISO 25217.

An environmental chamber was used for the tests at high temperature. A thermocouple was attached to the specimen in order to verify its real temperature. Once the temperature of the whole system achieved the desired set point, the set-up was kept at the target temperature for 1 hour to allow for the adhesive line reaching the same conditions.

The Version of Record of this manuscript has been published and is available in The Journal of Adhesion in press https://doi.org/10.1080/00218464.2019.1665519

For the ENF test, the 2L span was equal to 240 mm and a deflectometer was located in the middle of the specimen lower surface to measure the vertical displacement of the sample [12].

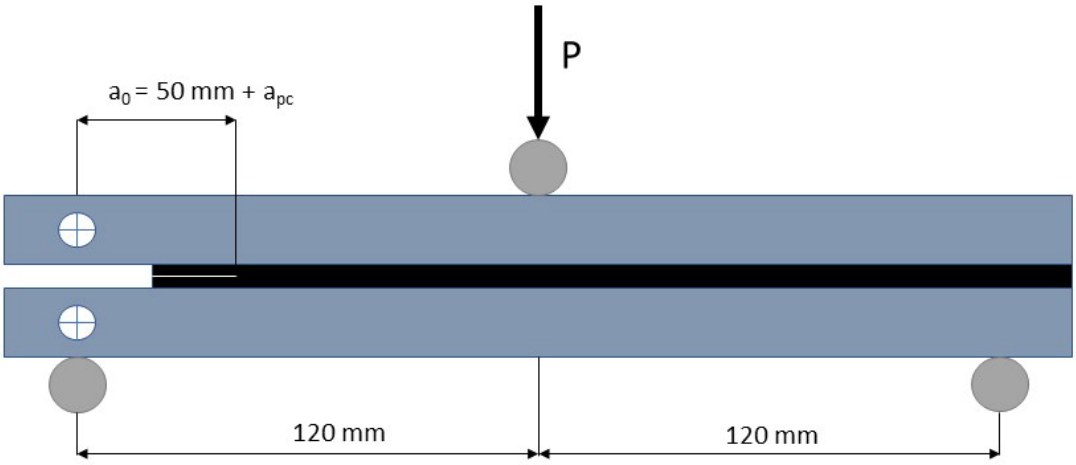

Figure 4: ENF test scheme ~~– adapted from [1]~~.

For all DCB and ENF samples, a pre-cracking test was performed. The same DCB set-up was used for the pre-cracking phase. Five DCB specimens and Four samples of ENF were tested for each temperature. Displacement and load were recorded in both test types.

2.3.1.1. Data reduction

For the DCB test, the Krenk's method of data reduction was used to determine G_{IC}, this method was well explained in a previous work by Cardamone *et al*. [12]. The Krenk's method for G_{IC} calculation considers the adhesive bonded line as a continuous distribution of springs in the middle of two simple beams. In special, this method takes into account

The Version of Record of this manuscript has been published and is available in The Journal of Adhesion in press https://doi.org/10.1080/00218464.2019.1665519

the rotation of the beams and the crack propagation is interpreted as a shortening of the adhesive length.

$$G_{IC} = \frac{Pa}{bEJ}\left(1 + \frac{1}{\lambda_\sigma a}\right)^2 \quad \text{Eq. 01}$$

where *J* is the single substrate moment of inertia, E - Young's modulus of the substrate, λ_σ - the bending stiffness of the beam, *b* – sample width, *P* – load and *a* – crack length.

For the ENF test the Compliance Based Beam Method (CBBM) proposed by de Moura et al. 2008 [22] was used for the G_{IIC} calculation, Eq. 2.

$$G_{IIC} = \frac{9P^2{a_e}^2}{16b^2E_f h^3} \quad \text{Eq. 02}$$

The variable a_e corresponds to the equivalent crack length accounting the effects of the process zone, E_f is the flexural modulus and h is the height of the substrate.

2.3.2. Single lap joint tensile test

SLJ were tested in an electro-mechanical tensile machine with a load cell of 60 KN. The tests at high temperatures were done using an environmental chamber to maintain the same temperature during the entire test, Fig. 5.

The Version of Record of this manuscript has been published and is available in The Journal of Adhesion in press https://doi.org/10.1080/00218464.2019.1665519

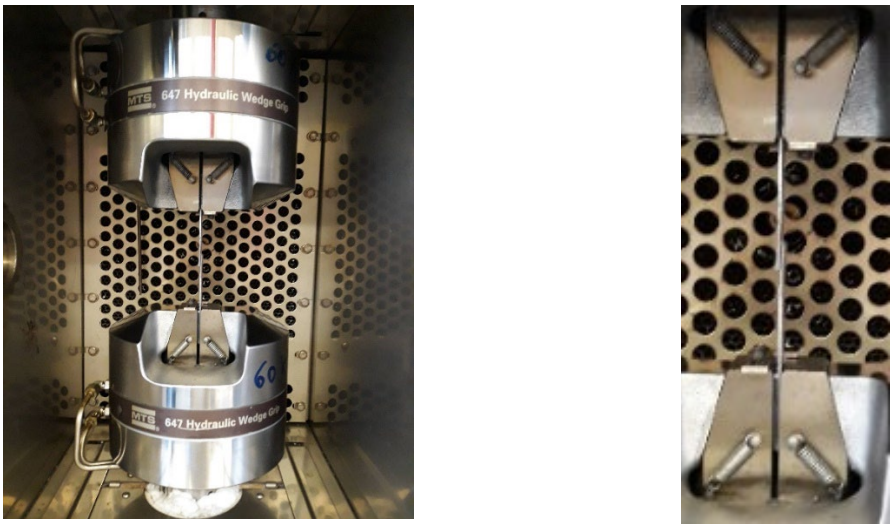

(a) (b)

Figure 5: (a) Tensile test of single lap joints and (b) detailed SLJ fixture.

A constant crosshead speed of 0.5mm/min was used for all the conditions. Five specimens were tested for each temperature. A thermocouple was used to measure the surface temperature of the sample. After the specimen achieved the required temperature, each specimen was kept in the chamber for other 30 minutes.

2.3.3. Bulk tensile test

Bulk tensile tests on the 7260 B/A epoxy adhesive were performed in the same electro-mechanical machine as for the single lap joints, with the same environmental chamber but equipped with a load cell of 10 kN. A constant crosshead speed of 1 mm/min was applied. An extensometer was used to record the strain in the gauge section of the specimen. Three specimens for each condition were tested.

The Version of Record of this manuscript has been published and is available in The Journal of Adhesion in press https://doi.org/10.1080/00218464.2019.1665519

3. EXPERIMENTAL RESULTS AND DISCUSSIONS

3.1. Bulk tensile tests

The 7260 B/A bulk samples were tested at room temperature, 40°C, 55°C and 70°C. For each specimen a stress-strain curve was obtained from the load and displacement data recorded by the testing machine. The representative stress/strain curves for each temperature can be observed in Fig. 6.

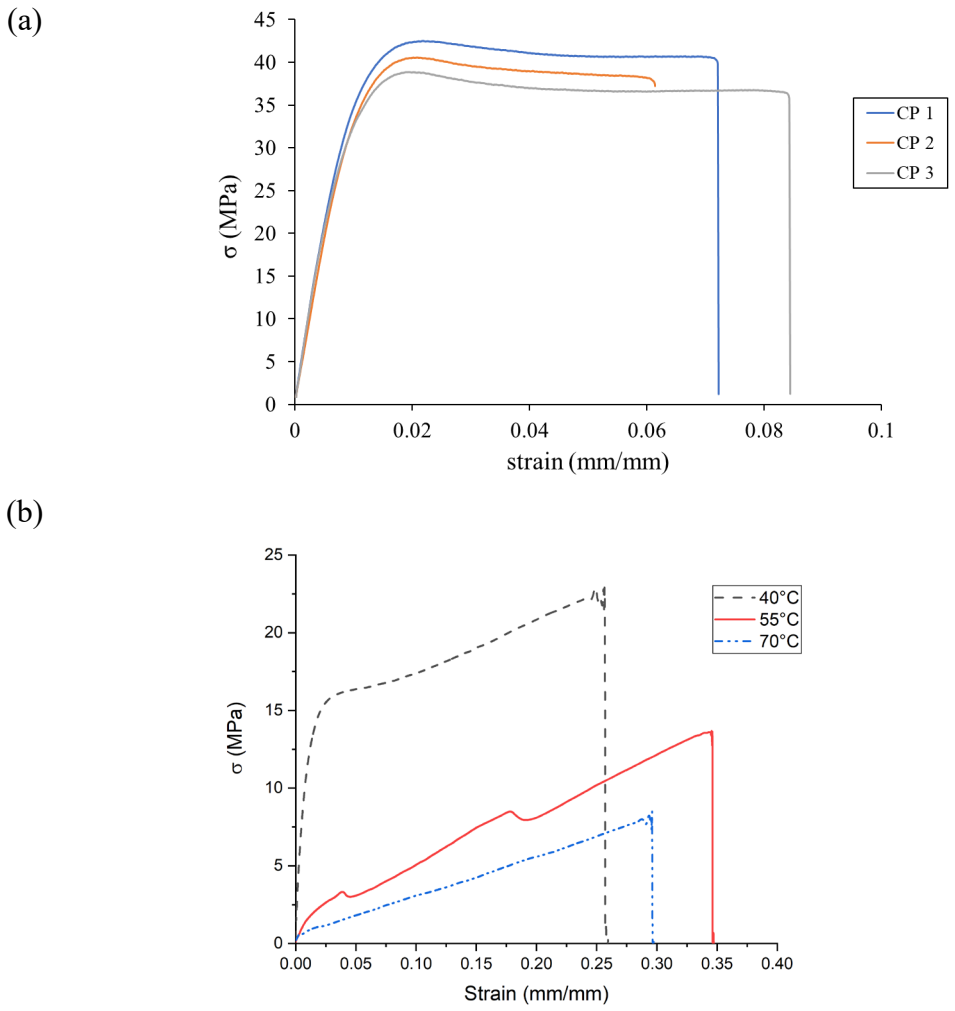

Figure 6: (a) Stress x strain at room temperature (b) Comparison of bulk mechanical behaviour as function of the temperature.

The Version of Record of this manuscript has been published and is available in The Journal of Adhesion in press https://doi.org/10.1080/00218464.2019.1665519

As can be seen in Figure 6 (a), the adhesive 7260 presents a ductile behaviour. In Figure 6 (b) it is possible to see an increase of the strain at failure and significant reduction of the maximum stress with the increase of the temperature.

The Young's modulus of the adhesive as function of the temperature was calculated by the secant method from the stress-strain curve, as recommended by the standard ISO 527. Table 3 summarizes the values of Young's modulus and maximum stress of the dogbone samples.

Table 3: Mechanical properties of the adhesive 3M Scotch-Weld™ 7260 B/A.

Temperature	20°C	40°C	55°C	70°C
Young's modulus (MPa)	4248 ± 297	1761 ± 254	191 ± 6.9	30.6 ± 3.8
Ultimate stress (MPa)	40.6 ± 1.5	22.9 ± 0.9	13.1 ± 0.8	7.2 ± 0.7

The variation of the temperature had a big impact on the Young's modulus. The elastic modulus presented a reduction of 58% and 95% at 40°C and 55°C, respectively. On the other hand, a moderate reduction of the ultimate tensile stress as function of the temperature, around 50% for each temperature step was recorded.

3.2. DCB tests

DCB results at room temperature were reported in Cardamone *et al*. [12]. DCB tests at 40°C, 55°C and 70°C were performed following the same procedure, with the addition of

The Version of Record of this manuscript has been published and is available in The Journal of Adhesion in press https://doi.org/10.1080/00218464.2019.1665519

an environmental chamber. One specimen at 40°C and 70 °C and three specimens at 55°C were tested. The representative curves of load versus displacement and the strain energy release rate for each condition are shown in the graphs of Figures 7 and 8, respectively.

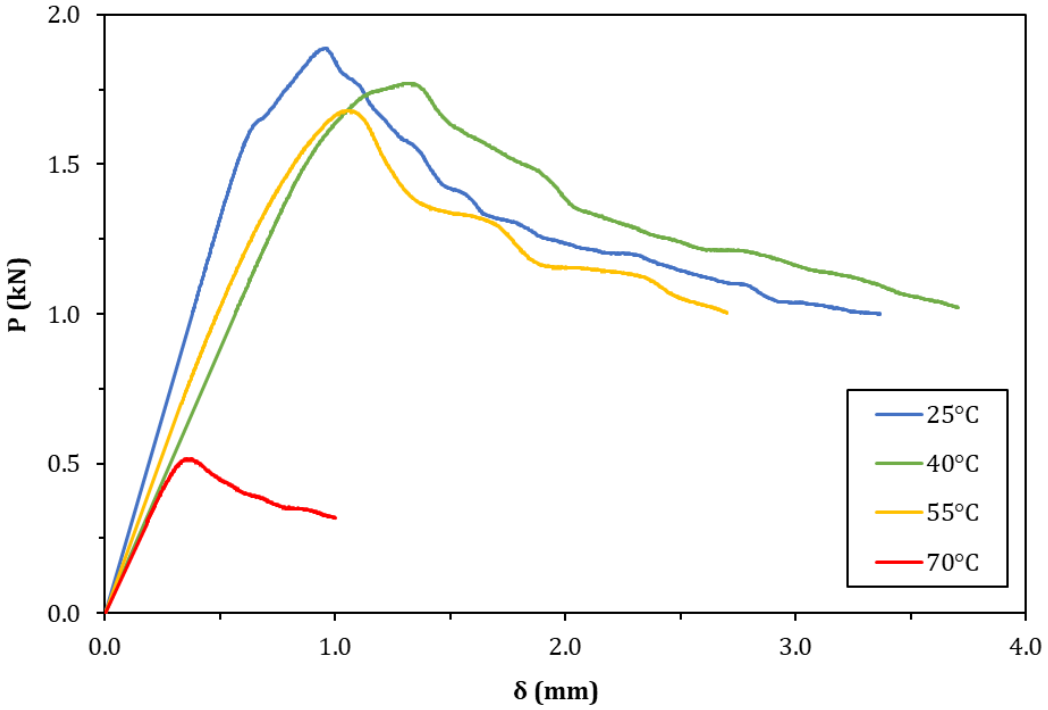

Figure 7: Experimental load vs. displacement of DCB tests on NS epoxy at different temperatures.

The Version of Record of this manuscript has been published and is available in The Journal of Adhesion in press https://doi.org/10.1080/00218464.2019.1665519

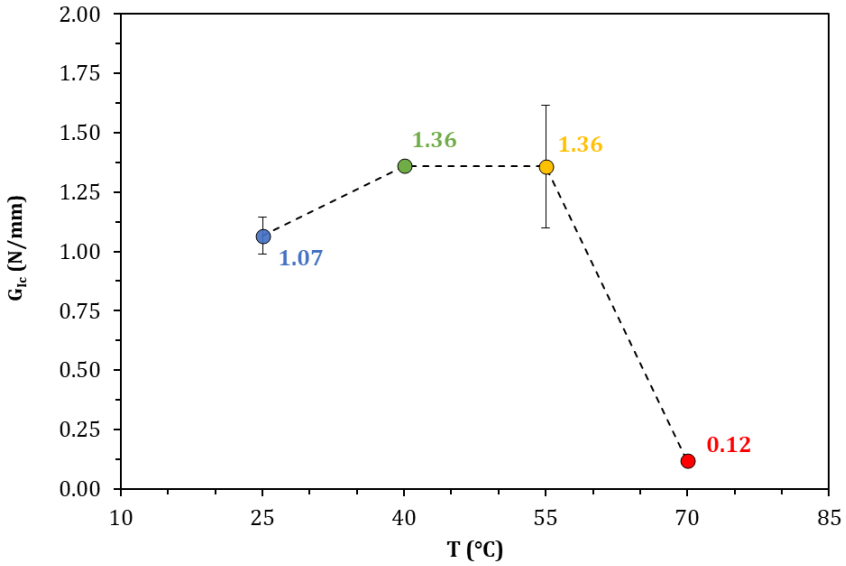

Figure 8: Strain energy release rate at different temperatures using the CBT data reduction method.

Figure 7 showcases the load-displacement curve for each temperature. It can be observed that the maximum load achieved during the test at 70°C is clearly reduced.

In Figure 8, the critical strain energy release rate presented the same average value at 40°C and 55°C, both slightly higher than that obtained at room temperature. Tests at the latter temperature showed a significant scatter of data. Conversely, the value achieved at 70°C (0.12 N/mm) showed a drop of about -89% of G_{Ic}, compared to that at RT.

Figure 9 presents the fracture mode of the studied samples. A cohesive fracture in the mid-plane of the adhesive bonding was experienced at RT and 40°C. Increasing the temperature, the failure mode switched from cohesive to adhesive.

The Version of Record of this manuscript has been published and is available in The Journal of Adhesion in press https://doi.org/10.1080/00218464.2019.1665519

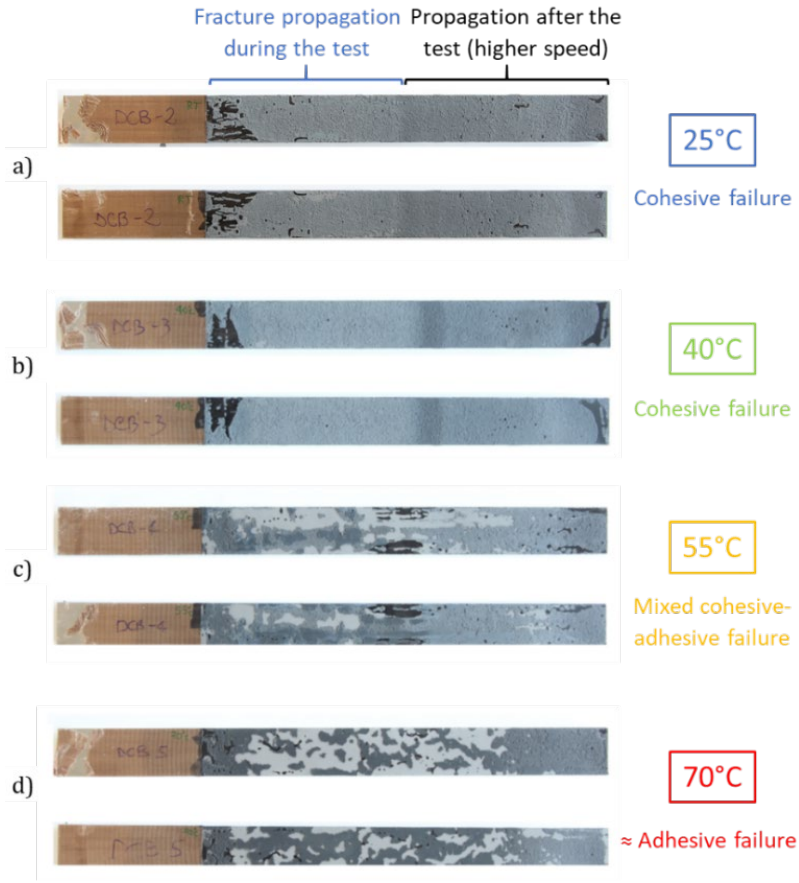

Figure 9: Fracture adhesive surface of DCB tests on NS epoxy at: a) RT; b) 40°C; c) 55°C; d) 70°C.

3.3. ENF tests

ENF results at room temperature can be found in Cardamone et al. [12]. ENF tests at 40°C, 55°C and 70°C were performed using an environmental chamber and the results are described in this section.

The representative curves of load versus displacement and the strain energy release rate in mode II for each condition are shown in the graphs of Figures 10 and 11, respectively.

The Version of Record of this manuscript has been published and is available in The Journal of Adhesion in press https://doi.org/10.1080/00218464.2019.1665519

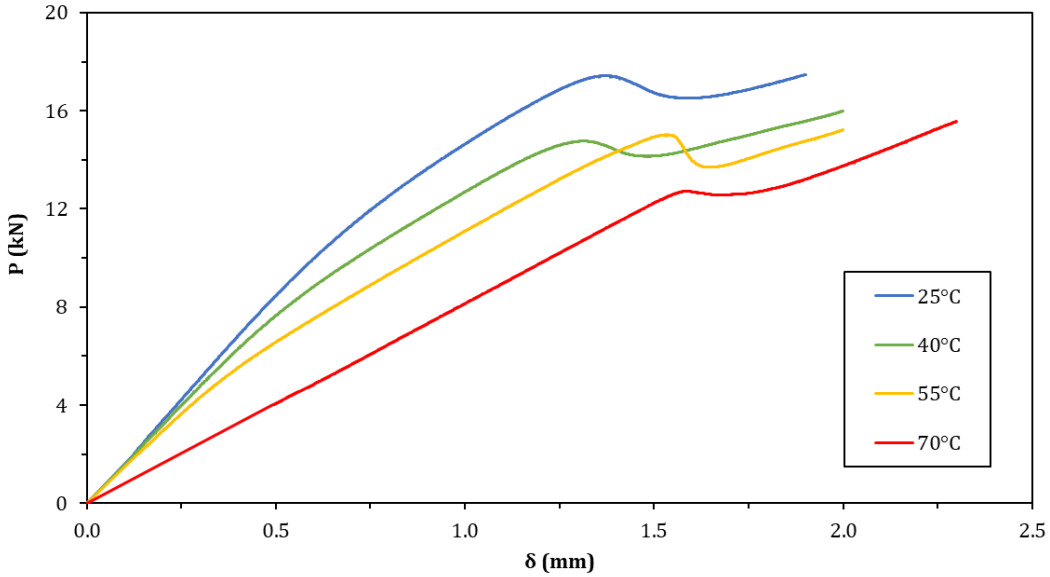

Figure 10: Experimental load vs. displacement of ENF tests on NS epoxy at different temperatures.

When the temperature increases, an interesting difference in the P-δ curves (Figure 10) can be observed. The first change in the slope value, experienced at RT approximately halfway before the load drop, occurred earlier as the temperature increased. Indeed, at 70°C this slope reduction even disappeared, and the P-δ curve continued almost linearly until the drop. This might indicate that a weaker mechanical behaviour of the adhesive was experienced as soon as the load was applied to the specimen.

The Version of Record of this manuscript has been published and is available in The Journal of Adhesion in press https://doi.org/10.1080/00218464.2019.1665519

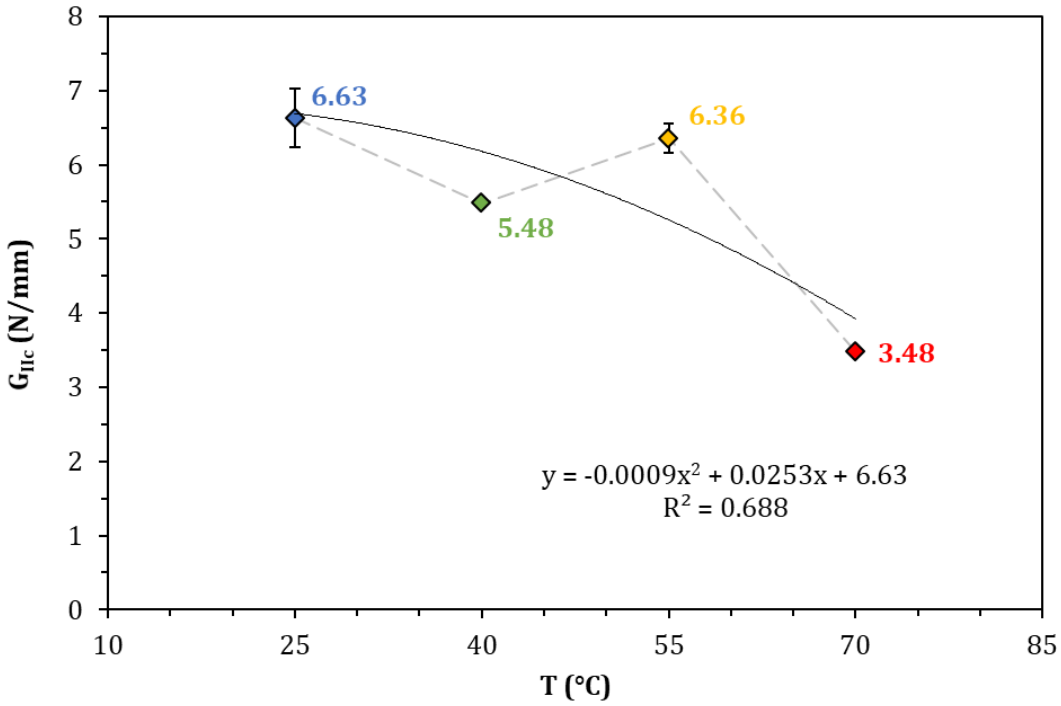

Figure 11: Mode II critical strain energy release rate of NS epoxy as a function of temperature.

For the mode II critical strain energy release rate (Figure 11) the reduction at 70°C is less than that observed for the critical energy in mode I.

The ENF failure modes are shown in Figure 12. Three zones are clearly recognizable for all specimens. The first cohesive fracture for few millimetres indicates the mode I pre-cracking stage and it allowed to accurately measure a_0. The second zone represents the mode II fracture propagation that did not occur fully in the mid-plane of the adhesive layer, as obtained in mode I, as at the micro-scale cracks in shear propagated in a zig-zag manner perpendicularly to the direction of max-principal stresses. In any case, a fully cohesive fracture was achieved at room temperature. The third zone corresponds to the mode I-

The Version of Record of this manuscript has been published and is available in The Journal of Adhesion in press https://doi.org/10.1080/00218464.2019.1665519

opening of the specimen at the end of the ENF tests, whose length allowed to accurately measure the effective total crack propagation and to compare it with that obtained by CBBM. Considering only the area of the crack propagation during the tests, the same phenomenon that happened for mode I occurred also in mode II testing. Increasing the test temperature, the failure mode switched from total cohesive to adhesive, and the fracture moved out from the adhesive mid-plane more pronouncedly than at RT.

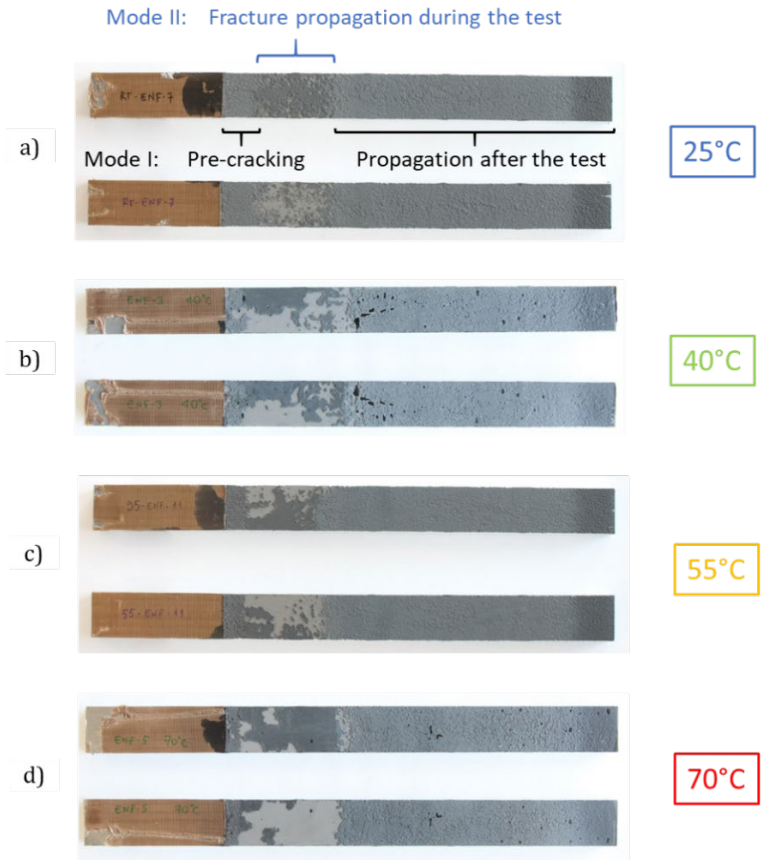

Figure 12: Fracture adhesive surface of ENF tests on NS epoxy at: a) RT; b) 40°C; c) 55°C; d) 70°C.

The Version of Record of this manuscript has been published and is available in The Journal of Adhesion in press https://doi.org/10.1080/00218464.2019.1665519

3.4. Single lap joints

At least 5 SLJ samples were tested at room temperature and high temperatures (40°C, 55°C and 70°C) in a universal tensile testing machine with a constant crosshead rate of 0.5 mm/min. The representative tensile curves of the SLJ specimens as function of the temperature are shown in Figure 13.

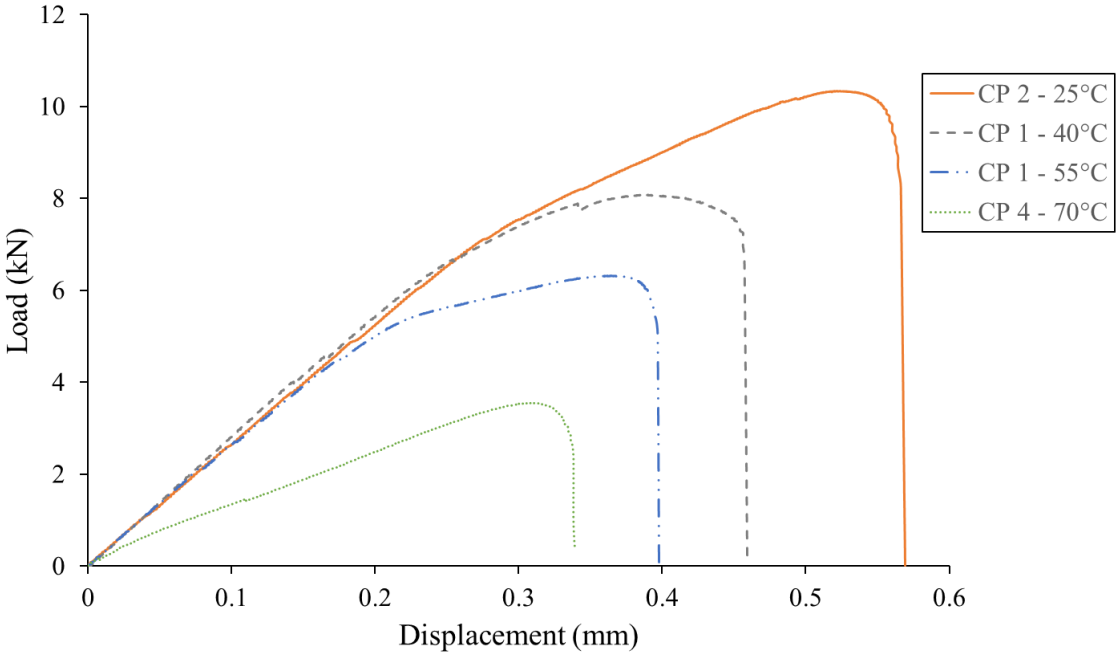

Figure 13: Representative load x displacement curves SLJ tests as function of temperature.

As can be seen in Figure 13, the maximum tensile load achieved at room temperature was around 11 kN. Increasing the temperature, a decrease of around 20% of the maximum load for each temperature step was observed.

The Version of Record of this manuscript has been published and is available in The Journal of Adhesion in press https://doi.org/10.1080/00218464.2019.1665519

The average lap shear strength as function of the temperature was calculated and it is presented in the graph of Figure 14, together with the displacement at failure.

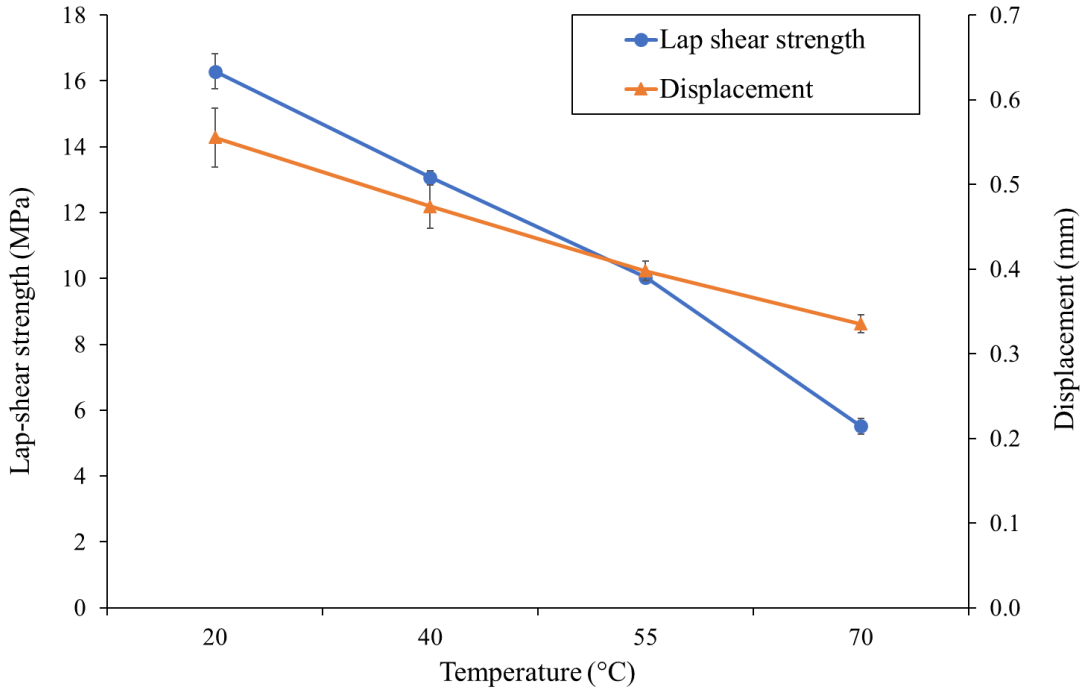

Figure 14: Average lap shear strength and displacement as a function of temperature.

With the increase of the temperature, a slight decrease of the lap shear strength was observed, from 16 MPa at room temperature to 10 MPa at 55°C. The reduction of the lap shear stress at 70°C was even more significant. This behaviour can be better understood by the analysis of the failure modes shown in Figure 15.

At room temperature and 40°C, the failure mode of the samples was fully cohesive. With the increase of the temperature a change in the failure mode from cohesive to completely adhesive was observed. At 55°C a thin layer cohesive failure and at 70°C an adhesive failure were observed.

The Version of Record of this manuscript has been published and is available in The Journal of Adhesion in press https://doi.org/10.1080/00218464.2019.1665519

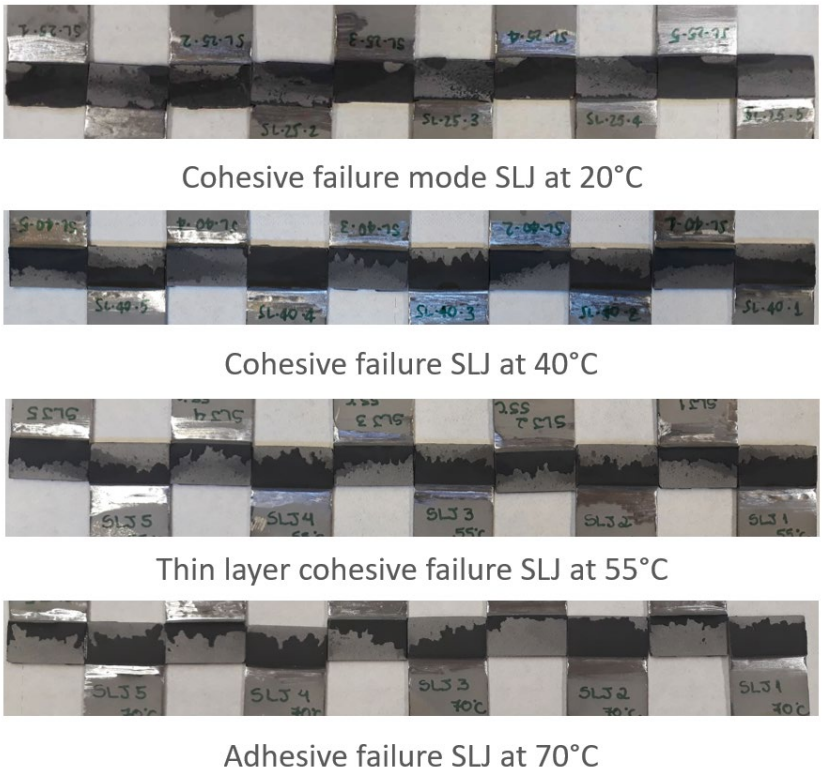

Figure 15: Failure modes SLJ as function of the temperature.

4. NUMERICAL MODELLING

Numerical optimizations were performed using the commercial software packages Abaqus™ and Isigth™, in order to identify the stiffness (e_I and e_{II}) and ultimate stress parameters (t_I and t_{II}) in tension and shear. Numerical analysis in pure mode I and mode II were done in Abaqus™, using a cohesive zone model. Then, numerical and experimental load versus displacement curves were matched by parameters optimization, i.e. by an error minimisation strategy set up in Isigth™.

After parameters identification, SLJ numerical analysis were performed to compare numerical prediction with the experimental behaviour. Given the fully adhesive behaviour

The Version of Record of this manuscript has been published and is available in The Journal of Adhesion in press https://doi.org/10.1080/00218464.2019.1665519

observed at 70°C, this case was not taken into consideration in this part of the work based on cohesive models.

4.1. Numerical modelling of mode I and II at different temperatures

A two-dimensional numerical modelling of the samples under pure mode I and II loading as function of the temperature was set up. Cohesive zone method with a bi-linear traction separation law and geometrical non-linearities was implemented to better represent the softening part of the adhesive and the deformations of the specimens.

As reasonable mesh sizes do not influence the strength prediction of CZM [23], a mesh with 1 mm x 1 mm elements was used. The numerical modelling details of the DCB and ENF tests were summarized in the table 4.

Table 4: Numerical modelling details of DCB and ENF tests.

	Substrate	Adhesive
Type of element (mesh)	CPS4R (Plane stress)	COH2D4
Elements global size	1	1
Element shape	Quadrangular	Quadrangular
Material model	Elastic – Perfectly plastic	Cohesive – Bi-linear TSL

Tie constrains were applied to connect the substrates and the adhesive through master and slave surface relationships. More details about the numerical modelling applied can be found in Cardamone *et al*. [12].

The Version of Record of this manuscript has been published and is available in The Journal of Adhesion in press https://doi.org/10.1080/00218464.2019.1665519

4.2. Numerical Optimization

The numerical optimization method implemented was the Hooke-Jeeves direct research, suitable for long running simulations and available in the Isigth™ software. The proposed optimization module determines the cohesive parameters by a local minimum identification through an iterative process (data matching between experimental/numerical loading – displacement curves in pure mode I and II) with a target function of minimizing the sum of the squared difference between experimental and numerical load values for the same displacement [12]:

$$f = \sum_{i=1}^{n} \left(P_i^{exp} - P_i^{sim}\right)^2 \qquad \text{Eq. 03}$$

4.2.1. Two free variables optimization

For these analyses the G_{IC} and G_{IIC} (from the DCB and ENF tests, respectively) parameters were set as fixed input parameters. On the other hand, the stiffness and ultimate tensile stress parameters, used in the bi-linear TSL for the numerical simulations, were selected as free variables. The results obtained by this optimization strategy can be seen in Table 5.

The Version of Record of this manuscript has been published and is available in The Journal of Adhesion in press https://doi.org/10.1080/00218464.2019.1665519

Table 5: Properties of the adhesive in function of the temperature.

Temperature	G_n^C (N/mm)	G_s^C (N/mm)	t_I^0(MPa)	t_{II}^0(MPa)	e_I (MPa/mm)	e_{II} (MPa/mm)
20°C	1.07	6.63	26.13	41.32	2114	19567
40°C	1.36	5.48	20.90	26.73	573	8553
55°C	1.36	6.36	20.21	17.90	1154	5408

The blue columns represent the parameters obtained by the two free variables optimization strategy. The ultimate strength in tension and shear (t_I^0 and t_{II}^0) presented reasonable behaviour as a function of the temperature in comparison with the experimental data obtained using bulk specimens, as with an increase of the temperature the ultimate strength decreased. On the other hand, the stiffness parameter presented an odd behaviour with temperature variations, as e_I values first decreased at 40°C and then increased again at 55°C.

4.2.2. One free variable optimization

In order to understand better, the influence of the stiffness parameter and its variation as a function of the temperature on the numerical simulations, another strategy was proposed, where only one free variable was defined.

In this case, other than the strain energy release rate for tension and shear conditions, also the stiffness parameter was set as a fixed parameter. The stiffness parameter is imposed as $e_I = E/t_a$ and $e_{II} = G/t_a$, E and G being the elastic moduli from the bulk tensile test

The Version of Record of this manuscript has been published and is available in The Journal of Adhesion in press https://doi.org/10.1080/00218464.2019.1665519

results. The ultimate tensile stress (t_I and t_{II}) was the free variable for this strategy. The optimization results can be found in table 6.

Table 6:Properties of the adhesive in function of the temperature.

Temperature	G_n^C (N/mm)	G_s^C (N/mm)	σ_u (MPa)	t_I^0 (MPa)	t_{II}^0 (MPa)	e_I (MPa/mm)	e_{II} (MPa/mm)
20°C	1.07	6.63	40.6	26.69	41.47	14159.5	10891.92
40°C	1.36	5.48	22.9	15.68	24.08	5869.9	4515.3
55°C	1.36	6.36	13.1	15.54	14.52	635.1	488.6

In this case the stiffness parameter presented a gradual reduction as function of the temperature, following the Young's modulus behavior, σ_u indicates the tensile ultimate stress of the bulk specimens at each temperature.

4.3. Numerical modelling of single lap joints at different temperatures

A two-dimensional model was used to predict the mechanical behaviour of the single lap joints. A CZM with a bi-linear traction separation law and non geometrical linearities were applied to the model. The substrates were modelled using plane strain eight-nodes quadrilateral solid elements with an elastic - perfectly plastic behaviour. Four – nodes cohesive elements were used for modelling the adhesive layer, as can be seen in Table 7.

The Version of Record of this manuscript has been published and is available in The Journal of Adhesion in press https://doi.org/10.1080/00218464.2019.1665519

Table 7: Numerical modelling details of SLJ tests.

	Substrate	Adhesive
Type of element (mesh)	CPE8R	COH2D4
Elements global size	0.3	0.3
Element shape	Quadrangular	Quadrangular
Material model	Elastic – Perfectly plastic	Cohesive – Bi-linear TSL

A tie constrain was used to link the substrates to the adhesive. For these analyses, a spring element was added at the end of the specimen to account for the compliance of the testing machine. The spring stiffness was determined by best fitting the experimental results at RT and was equal to 60000 N/mm. The boundary conditions applied, and the spring element can be seen in Figure 16.

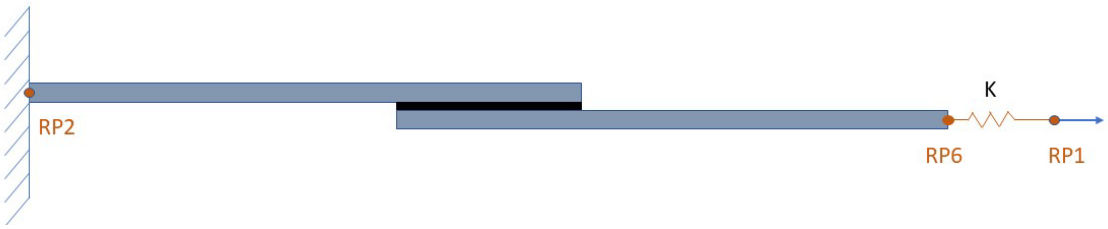

Figure 16: SLJ boundary conditions.

In Figures 16, it is possible to see the reference points RP1, RP2 and RP6. The orange line between RP1 and RP6 represents the spring. The RP2 represents the clamping of the sample in the tensile machine and the RP1 is the point where a horizontal constant displacement is applied and restraining in the vertical direction.

The Version of Record of this manuscript has been published and is available in The Journal of Adhesion in press https://doi.org/10.1080/00218464.2019.1665519

The finite element analyses were carried out implementing three different sets of the cohesive parameters for the bilinear traction separation law: the properties from the bulk specimens and from the two optimization strategies. The comparison between experimental and numerical curves for each group of cohesive parameters at room temperature can be seen in Figure 17.

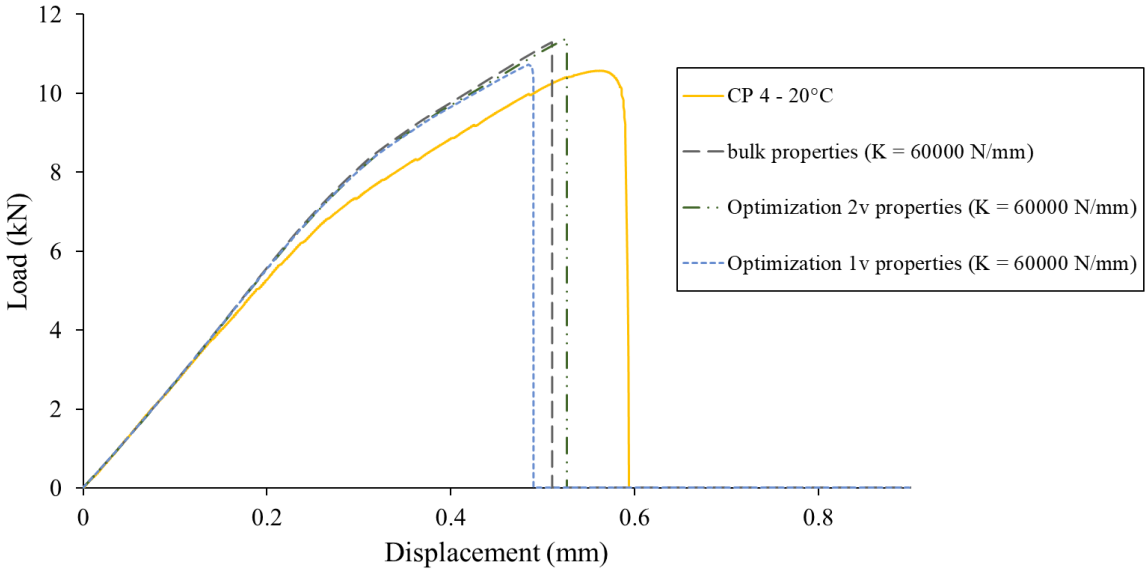

Figure 17: Representative load x displacement curves SLJ tests (numerical and experimental results).

Figure 17 shows that all the strategies presented a good accuracy with respect to the prediction of the maximum load of the SLJ at room temperature. The one free variable strategy allowed the best agreement, as it predicted a maximum load only 2% higher than the experimental one. By all the methods, the displacement at failure was underestimated by 0.1 mm. The process was repeated for all the test temperatures. Values of the maximum load and displacement at failure are reported in the graph of Figures 18 and 19.

The Version of Record of this manuscript has been published and is available in The Journal of Adhesion in press https://doi.org/10.1080/00218464.2019.1665519

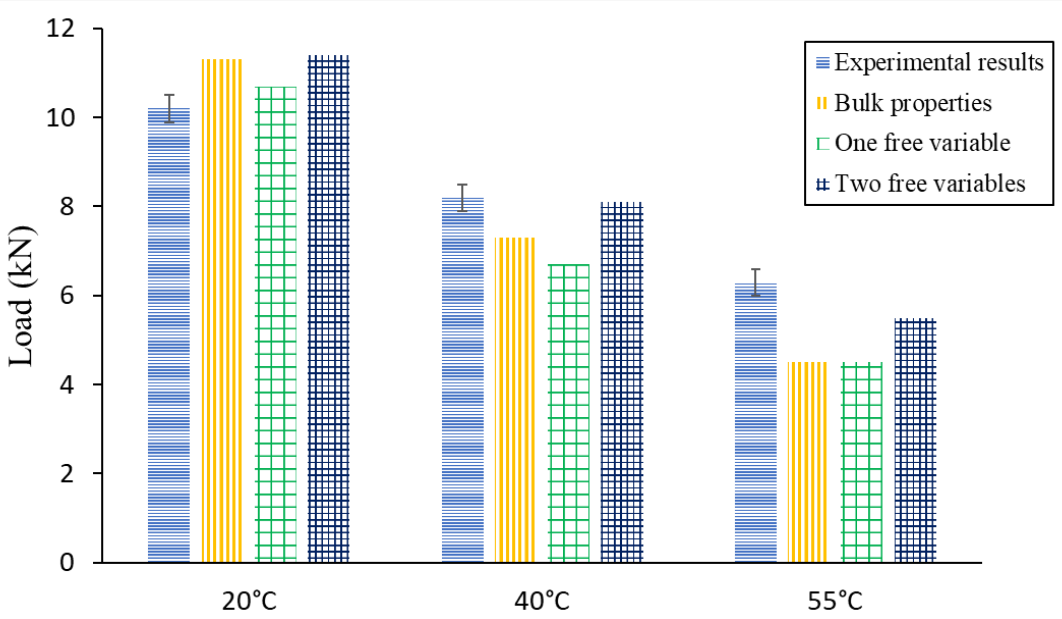

Figure 18:Comparison of load carried out by numerical modelling.

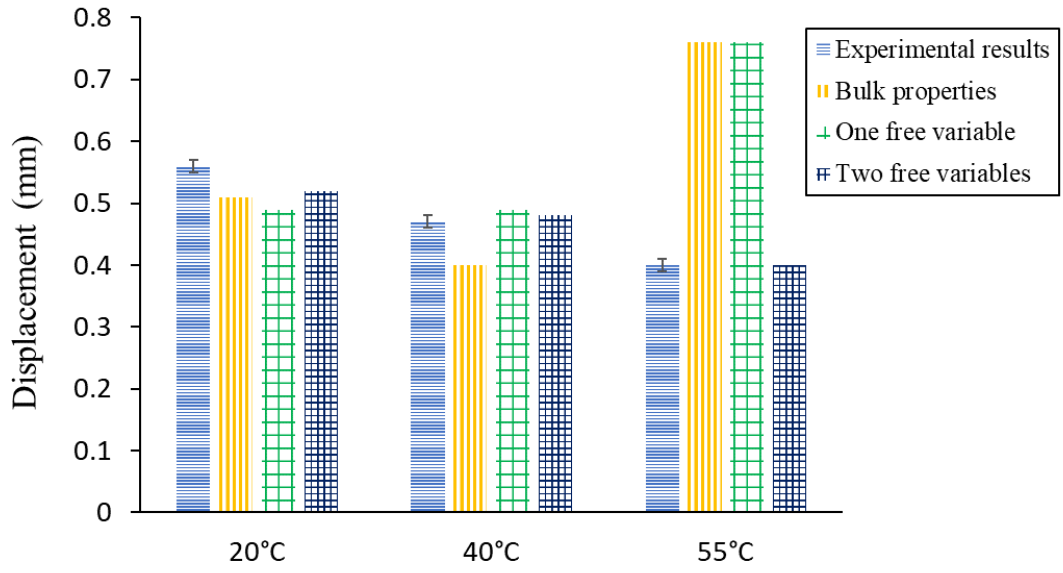

Figure 19: Comparison of ~~load~~ displacement at failure carried out by numerical modelling.

As it can be seen in Figures 18 e 19, the load and displacement predictions at high temperatures (40 and 55°C) were more accurate using the optimization method with two

The Version of Record of this manuscript has been published and is available in The Journal of Adhesion in press https://doi.org/10.1080/00218464.2019.1665519

free variables. Particularly, at 55°C the numerical method using bulk properties as the cohesive parameters and the optimization method of one free variable presented similar values and an error of 28% for the load prediction and an over prediction of 90% for the displacement.

At 55°C the adhesive started to change its failure method from completely cohesive to thin layer cohesive failure, followed by an adhesive failure at 70°C. For this reason, no cohesive modelling of the SLJ was attempted for the 70°C case. The adhesive at room temperature showed a ductile behaviour and at 55°C its plastic behaviour was increased. Under these circumstances, the elastic properties and, consequently, the stiffness parameter should become less relevant for the numerical results. In facts, according to Rocha *et al*. [23], the influence of the stiffness parameter on the CZM is reduced in ductile adhesives due to plasticisation phenomena and absence of sharp peak stresses at the overlap ends.

For this specific adhesive and environmental conditions, the two free variables optimization method appears to be more suitable for accurate prediction of the maximum load and the displacement at failure of SLJ, if a bilinear TSL is adopted like in the previous work [12], where the bilinear TSL appeared to allow to reproduce accurately the behaviour of joints at RT. However, the more dominant plastic behaviour of the adhesive observed at higher temperatures reported in this work indicates that the CZM based on a bilinear law has limitations that could probably be overcome by changing the shape of the TSL. Therefore, future developments will explore other shapes of the TSL and will focus on the

The Version of Record of this manuscript has been published and is available in The Journal of Adhesion in press https://doi.org/10.1080/00218464.2019.1665519

relationship between the plastic behaviour of the adhesive observed in bulk tests and cohesive modelling.

5. CONCLUSIONS

This work analysed the temperature effects on the mechanical behaviour of the 7260 B/A non-sag epoxy adhesive. Four types of mechanical tests were performed at different temperatures (20, 40, 55 and 70°C): DCB, ENF, SLJ and bulk tensile test. The bulk tensile test in function of the temperature showed that the adhesive at room temperature presents a ductile behaviour and with the increase of the temperature a reduction of its elastic properties, as well as of its ultimate tensile strength, was observed.

During the DCB, ENF and SLJ tests, it was noticed that the adhesive at 55 and 70°C changes failure behaviour from cohesive failure to completely adhesive failure.

The parameters of a bilinear TSL were identified according to three different strategies: cohesive parameters equal to tensile properties form bulk specimens, DCB and ENF data matching with two free variables, DCB and ENF data matching with one free variable.

The different TSL parameter sets were used to model the tensile behaviour of SLJ tested at the same temperatures as the DCB and ENF specimens. The two free variables optimization strategy achieved the highest accuracy in predicting the value of the load and the displacement at failure.

Future developments will focus on the influence of the ductility of the adhesive and of the shape of the TSL on the accuracy of the numerical models.

The Version of Record of this manuscript has been published and is available in The Journal of Adhesion in press https://doi.org/10.1080/00218464.2019.1665519

REFERENCES

[1] Banea, M. D.; Rosioara, M.; Carbas, R. J. C.; da Silva, L. F. M. Multi-material adhesive joints for automotive industry. *Compos. Part B Eng.* **2018**, 151, 71-77. DOI: **10.1016/j.compositesb.2018.06.009**.

[2] Marques, E. A. S.; da Silva, L. F. M.; Banea, M. D.; Carbas, R. J. C. Adhesive joints for low- and high-temperature use: An overview. *J. Adhes.* **2014**, 91, 556-585. DOI: **10.1080/00218464.2014.943395**.

[3] Avendaño, R.; Carbas, R. J. C.; Marques, E. A. S.; da Silva, L. F. M.; Fernandes, A. A. Effect of temperature and strain rate on single lap joints with dissimilar lightweight adherends bonded with an acrylic adhesive. *Compos. Struct.* **2016**, 152, 34-44. DOI: **10.1016/j.compstruct.2016.05.034**.

[4] Deb, A.; Malvade, I.; Biswas, P.; Schroeder, J. An experimental and analytical study of the mechanical behaviour of adhesively bonded joints for variable extension rates and temperatures. *Int. J. Adhes. Adhes.* **2008**, 28, 1–2. DOI: **10.1016/j.ijadhadh.2007.02.004**.

[5] Carlberger, T.; Biel, A.; Stigh, U. Influence of temperature and strain rate on cohesive properties of a structural epoxy adhesive. *Int. J. Fract.* **2009**, 155, 155 - 166. DOI: **10.1007/s10704-009-9337-4**.

[6] Banea M. D.; da Silva, L. F. M. The effect of temperature on the mechanical properties of adhesives for the automotive industry. *J. Mater. Design and Appl.* **2010**, 224, 56 - 62. DOI: **10.1243/14644207JMDA283**.

[7] Banea, M. D.; da Silva, L. F. M.; Carbas, R.; de Barros, S. Effect of Temperature and Moisture on the Tensile Properties of a TEPs-Modified Adhesive, *Mater. Plast.* **2018**, 55, 478 - 481.

[8] de Sousa, C. C. R. G.; Campilho, R.; Marques, E. A. S.; Costa, M.; da Silva, L. F. M. Overview of different strength prediction techniques for single-lap bonded joints, *J. Mater. Design and Appl.* **2017**, 231, 1–2. DOI: **10.1177/1464420716675746**.

[9] Banea, M. D.; da Silva, L. F. M.; Campilho, R. D. S. G.; de Jesus, A. M. P. Characterization of Aluminium Single-Lap Joints for High Temperature

The Version of Record of this manuscript has been published and is available in The Journal of Adhesion in press https://doi.org/10.1080/00218464.2019.1665519

Applications, *Mater. Sci. Forum* **2012**, 730, 721-726. DOI: **10.4028/www.scientific.net/msf.730-732.721**.

[10] Banea, M. D.; da Silva, L. F. M.; Campilho, R. D. S. G. Effect of temperature on tensile strength and mode I fracture toughness of a high temperature epoxy adhesive, *J. Adhes. Sci. Tech.* **2012**, 26, 939-953. DOI: **10.1163/156856111X593649**.

[11] Viana, G.; Machado, J.; Carbas, R.; Costa, M.; da Silva, L. F. M.; Vaz, M.; Banea M. D. Strain rate dependence of adhesive joints for the automotive industry at low and high temperatures, *J. Adhes. Sci. Tech.* **2018**, 32, 2162–2179. DOI: **10.1080/01694243.2018.1464635**.

[12] Cardamone, S.; Bernasconi, A.; Giglio, M. Characterization of the 3M Scotch-Weld™ 7260 B/A epoxy adhesive by cohesive damage models and application to a full-scale bonded sub-structure. *J. Adhes.* **2019**, 1545-5823. DOI: **10.1080/00218464.2019.1591278**.

[13] Banea, M. D.; da Silva, L. F. M.; Campilho, R. D. S. G. Effect of temperature on the shear strength of aluminium single lap bonded joints for high temperature applications, *J. Adhes. Sci. Tech.* **2014**, 28, 1367-1381. DOI: **10.1080/01694243.2012.697388**.

[14] Banea, M. D.; da Silva, L. F. M.; Campilho, R. D. S. G. Mode II fracture toughness of adhesively bonded joints as a function of temperature: Experimental and numerical study, *J. Adhes.* **2012**, 88, 534-551. DOI: **10.1080/00218464.2012.660835**.

[15] Fernandes, R. L.; de Moura, M. F. S. F.; Moreira, R. D. F. Effect of temperature on pure modes I and II fracture behavior of composite bonded joints, *Compos. Part B Eng.* **2016**, 96, 35-44. DOI: **10.1016/j.compositesb.2016.04.022**.

[16] Charalambous, G.; Allegri, G.; Hallett, S. R. Temperature effects on mixed mode I/II delamination under quasi-static and fatigue loading of a carbon/epoxy composite, *Compos. Part A Appl. Sci. Manufact.* **2015**, 77, 75-86. DOI: **10.1016/j.compositesa.2015.05.016**.

[17] He, X. A review of finite element analysis of adhesively bonded joints, *Int. J. Adhes. Adhes.* **2011**, 31, 248-264. DOI: **10.1016/j.ijadhadh.2011.01.006**.

The Version of Record of this manuscript has been published and is available in The Journal of Adhesion in press https://doi.org/10.1080/00218464.2019.1665519

[18] Campilho, R. D. S. G.; Fernandes, T. A. B. Comparative Evaluation of Single-lap Joints Bonded with Different Adhesives by Cohesive Zone Modelling, *Proc. Eng.* **2015**, 114, 102-109. DOI: **10.1016/j.proeng.2015.08.047**.

[19] Campilho, R. D. S. G.; Banea, M. D.; Neto, J. A. B. P.; da Silva, L. F. M. Modelling adhesive joints with cohesive zone models: Effect of the cohesive law shape of the adhesive layer, *Int. J. Adhes. Adhes.* **2013**, 44, 48-56. DOI: **10.1016/j.ijadhadh.2013.02.006**.

[20] Campilho, R. D. S. G.; Banea, M. D.; Neto, J. A. B. P.; da Silva, L. F. M. Modelling of single-lap joints using cohesive zone models: Effect of the cohesive parameters on the output of the simulations, *J. Adhes.* **2012**, 88, 513-533. DOI: **10.1080/00218464.2012.660834**.

[21] Gustafson P. A.; Waas, A. M. The influence of adhesive constitutive parameters in cohesive zone finite element models of adhesively bonded joints, *Int. J. Solids Struct.* **2009**, 46, 2201-2215. DOI: **10.1016/j.ijsolstr.2008.11.016**.

[22] de Moura, M. F. S. F.; Gonçalves, J. P. M.; Chousal, J. A. G.; Campilho, R. D. S. G. Cohesive and continuum mixed-mode damage models applied to the simulation of the mechanical behaviour of bonded joints, *Int. J. Adhes. Adhes.* **2008**, 28, 419-426. DOI: **10.1016/j.ijadhadh.2008.04.004**.

[23] Rocha, R. J. B.; Campilho, R. D. S. G. Evaluation of different modelling conditions in the cohesive zone analysis of single-lap bonded joints, *J. Adhes.* **2018**, 94, 562-582. DOI: **10.1080/00218464.2017.1307107**.

[24] Belnoue, J. P. H.; Hallett, S. R. Cohesive/adhesive failure interaction in ductile adhesive joints Part I: A smeared-crack model for cohesive failure, *Int. J. Adhes. Adhes.* **2016**, 68, 359-368. DOI: **10.1016/j.ijadhadh.2016.03.009**.

[25] Jia, D; Zheng, J.; Chen, X.; Yu, J. Modeling the temperature-dependent mode I fracture behavior of adhesively bonded joints, *J. Adhes.* **2017**, 93, 481-503. DOI: **10.1080/00218464.2015.1093938**.

[26] Qin, G.; Na, J.; Tan, W.; Mu, W.; Ji, J. Failure prediction of adhesively bonded CFRP-Aluminium alloy joints using cohesive zone model with consideration of temperature effect, *J. Adhes.* **2019**, 95, 723-746. DOI: **10.1080/00218464.2018.1440212**.